

## Cross sections and spin polarizations for $e^\pm$ scattering from cadmium

Sultana N. Nahar

*Department of Astronomy, The Ohio State University, Columbus, Ohio 43210*

(Received 19 April 1990; revised manuscript received 17 October 1990)

Various scattering cross sections such as differential, integrated-elastic, momentum-transfer, and total cross sections, and the spin-polarization parameters for both the elastic and the total scatterings of electrons and positrons from cadmium atoms in the impact-energy range of 6.4–300 eV, have been calculated relativistically by solving the Dirac equation. For the pure elastic-scattering case, the projectile-target interaction is represented by a real model potential that includes the static potential (attractive), a parameter-free polarization potential (attractive) and an electron-exchange potential for the electrons scattering, and the static potential (repulsive) and a parameter-free polarization potential (attractive) different from that of electrons scattering for the positrons scattering from cadmium. For the total scattering, which includes both the elastic-scattering and the inelastic-scattering processes, the total interaction is represented by a complex potential by adding a model absorption potential as its imaginary part. It has been observed that the agreement of the calculated differential cross section (DCS) curves for the elastic scattering of electrons from cadmium is reasonable with the previously measured values of DCS while the agreement is good with the recently measured values of DCS.

### I. INTRODUCTION

A few investigations have been made recently of electrons scattering from cadmium to obtain the scattering features of this comparatively heavy atom ( $Z=48$ ). Experiments have been performed by Nogueira, Newell, and Johnstone,<sup>1</sup> Marinkovic *et al.*,<sup>2</sup> and Marinkovic<sup>2</sup> to measure the differential cross sections at various impact energies for electrons scattering from cadmium. Theoretical calculations for both the electron and positron elastic scattering from cadmium have been made by Pangantiwar and Srivastava.<sup>3</sup> In their calculation, they used an optical real model potential to obtain the differential and the integrated cross sections for the elastic scattering. The present relativistic calculation has been carried out by solving the Dirac equation for both the elastic scattering and the total scattering of electrons and positrons from cadmium in the impact-energy range of 6.4–300 eV. The projectile-target interaction  $V(r)$  has been represented by a real model potential  $V_R(r)$  to obtain elastic scattering (differential, integrated-elastic, and momentum-transfer) cross sections and the various spin-polarization parameters for the elastic scattering of electrons and the positrons from cadmium. Then  $V(r)$  has been represented by a complex model potential  $V_R(r) + iV_A(r)$  by adding a model absorption potential  $V_A(r)$  as its imaginary part to obtain the same cross sections and spin polarizations for the elastic scattering along with the total cross sections.

### II. THEORY

#### A. Interaction potentials

The total projectile-target interaction potential can be expressed as

$$V(r) = V_R(r) + iV_A(r), \quad (1)$$

where use of only the real part  $V_R(r)$  for  $V(r)$  accounts for the pure elastic scattering and inclusion of the absorption potential  $V_A(r)$  gives the total scattering that includes both the elastic-scattering and the inelastic-scattering processes such as excitation, ionization, recombination, etc. causing an absorption in the scattered beam.

In the present calculation  $V_R$  is represented by a model potential that consists of

$$V_R(r) = \begin{cases} V_S(r) + V_{p^-}(r) + V_{ex}(r) & \text{for electrons scattering.} \\ V_S(r) + V_{p^+}(r) & \text{for positrons scattering.} \end{cases} \quad (2a)$$

(2b)

$V_S(r)$ , which is attractive for electrons scattering and repulsive for positrons scattering, is the static potential of projectile and is obtained by averaging over the target wave function as

$$\begin{aligned} V_S(r) &= \int |\psi_T(\mathbf{r}_1, \dots, \mathbf{r}_Z)|^2 \\ &\quad \times \left[ \frac{Zee_p}{r} - ee_p \sum_{i=1}^Z \frac{1}{|\mathbf{r} - \mathbf{r}_i|} \right] d\mathbf{r}_1 \dots d\mathbf{r}_Z \\ &= \frac{Zee_p}{r} - ee_p \sum_n \sum_l \sum_m N_{nlm} \int |\Phi_{nlm}(\mathbf{r})|^2 \frac{1}{|\mathbf{r} - \mathbf{r}'|} d\mathbf{r}', \end{aligned} \quad (3)$$

where  $\psi_T$  is the antisymmetric Hartree-Fock target wave function and the  $\Phi_{nlm}(\mathbf{r})$ 's are the spatial atomic orbitals,  $e_p$  is the projectile charge and  $N_{nlm}$  is the occupancy

number of the orbit ( $n, l, m$ ). In the present calculation, the radial part  $\phi(r)$  of the orbital  $\Phi_{nlm}(\mathbf{r}) = \phi_{nl}(r)Y_{lm}(\hat{\mathbf{r}})$  is expanded in terms of Slater-type orbitals given in the tables of Clementi and Roetti.<sup>4</sup>  $V_{p\pm}(r)$  are the parameter-free polarization potentials for the positrons and electrons scattering from cadmium, respectively. Depending on the location of the projectile from the target,  $V_{p\pm}(r)$  has two forms, the short range and the long range, as<sup>5,6</sup>

$$V_{p\pm}(r) = \begin{cases} V_{\text{SR}\pm}(r) & \text{for } r < r_c \\ V_{\text{LR}}(r) & \text{for } r \geq r_c, \end{cases} \quad (4)$$

where  $r_c$  is the point where the two forms cross each other for the first time. The short-range form for the *electrons scattering* based on the free-electron gas exchange potential is given by<sup>5</sup>

$$V_{\text{SR}-}(r) = \begin{cases} 0.0622 \ln r_s - 0.096 + 0.018 r_s \ln r_s - 0.02 r_s, & r_s \leq 0.7 \\ -0.1231 + 0.03796 \ln r_s, & 0.7 < r_s \leq 10 \\ -0.876 r_s^{-1} + 2.65 r_s^{-3/2} - 2.8 r_s^{-2} - 0.8 r_s^{-5/2}, & 10 \leq r_s \end{cases} \quad (5)$$

and for the *positrons scattering* by<sup>6</sup>

$$V_{\text{SR}+}(r) = \begin{cases} [-1.82/\sqrt{r_s} + (0.051 \ln r_s - 0.115) \ln r_s + 1.167]/2 & \text{for } r_s < 0.302 \\ (-0.92305 - 0.09098/r_s^2)/2 & \text{for } 0.302 \leq r_s \leq 0.56 \\ [-8.7674 r_s (r_s + 2.5)^{-3} + (-13.151 + 0.9552 r_s)(r_s + 2.5)^{-2} + 2.8655(r_s + 2.5)^{-1} - 0.6298]/2 & \text{for } 0.56 \leq r_s \leq 8.0, \end{cases} \quad (6)$$

where  $r_s = \{3/[4\pi\rho(\mathbf{r})]\}^{1/3}$ ,  $\rho(\mathbf{r})$  is the undistorted electronic density of the target, which for the spherically symmetric cadmium atom is given by

$$\rho(\mathbf{r}) = \frac{1}{4\pi} \sum_n \sum_l N_{nl} |\phi_{nl}(r)|^2, \quad (7)$$

where  $N_{nl}$  is the occupancy number of the orbital ( $n, l$ ). The long-range form of both  $V_{p\pm}(r)$  is given by

$$V_{\text{LR}}(r) = -\alpha_d/2r^4, \quad (8)$$

where  $\alpha_d$  is the static electric dipole polarizability. For the present calculation it is taken to be 43.7.<sup>3</sup> The exchange potential  $V_{\text{ex}}(r)$  due to exchange between the projectile electron and atomic electrons of the target is given by<sup>7</sup>

$$V_{\text{ex}}(r) = \frac{1}{2} \{ [E - V_D(r)] - [(E - V_D)^2 + \rho(r)]^{1/2} \}, \quad (9)$$

where  $V_D = V_S + V_{p-}$  is the direct interaction potential and  $\rho(r)$  is the radial density of the target.

The impact-energy range considered in the present calculation exceeds the threshold energy (3.734 eV for the first excitation<sup>8</sup>) of inelastic electrons scattering as well as the threshold energy (2.191 eV for the positronium formation<sup>8</sup>) of the inelastic positron scattering from cadmium and hence causes an absorption in the scattered beam. To include the absorption in the scattered beam, version 3 of the semiempirical model absorption potential of Staszewska, Schwenke, and Truhlar,<sup>9</sup>

$$V_A = -\frac{1}{2} v \rho(\mathbf{r}) \bar{\sigma}_b, \quad (10)$$

for the electron scattering has been used in the present work. In Eq. (10),  $v = [2(E - V_R)/m_0]^{1/2}$  is the local velocity of the projectile for  $(E - V_R) \geq 0$  and  $\bar{\sigma}_b$  is the

average quasifree binary collision cross section obtained nonempirically by using the free-electron gas model for the target. The forms of the two parameters  $\alpha$  and  $\beta$  introduced in  $\bar{\sigma}_b$  depend on the threshold energy and the ionization potential and are obtained empirically.<sup>9</sup> The factor  $\frac{1}{2}$  in Eq. (10) is introduced to account for the exchange between the incident electron and the atomic electrons of the target. The same absorption potential can be used for the positron scattering also with the factor of  $\frac{1}{2}$  replaced by 1 since there is no exchange effect during the positron scattering.

## B. Cross sections and spin polarizations

The Dirac equation for a projectile of rest mass  $m_0$  traveling in a central field  $V(r)$  at a velocity  $\mathbf{v}$  is given by

$$[c\boldsymbol{\alpha} \cdot \mathbf{p} + \beta m_0 c^2 + V(r)]\psi = E\psi, \quad (11)$$

where  $E = m_0 \gamma c^2 = E_i + m_0 c^2$  is the total energy,  $\gamma = (1 - v^2/c^2)^{-1/2}$ , and  $E_i$  is the impact kinetic energy of the projectile. The operators  $\boldsymbol{\alpha}$  and  $\beta$  in Eq. (11) are expressed by the usual  $4 \times 4$  Dirac matrices.<sup>10</sup> The spinor  $\psi$  has four components,  $\psi = (\psi_1, \psi_2, \psi_3, \psi_4)$ , where  $(\psi_1, \psi_2)$  are the large components and  $(\psi_3, \psi_4)$  are the small components of  $\psi$ . For a central potential, the above equation can be reduced to a set of two equations similar to the form of the Schrödinger equation as<sup>11</sup>

$$g_l^{\pm'''} + \left[ K^2 - \frac{l(l+1)}{r^2} - U_l^{\pm}(r) \right] g_l^{\pm}(r) = 0, \quad (12)$$

where  $g_l^{\pm}$  is related to the radial part  $G_l^{\pm}$  of the large component of  $\psi$  as  $G_l = \sqrt{\eta} g_l / r$ ,  $\eta = (E - V + m_0 c^2)/c\hbar$ , and  $K^2 = (E^2 - m_0^2 c^4)/\hbar^2 c^2$ . The effective Dirac poten-

tial terms  $U_l^\pm$  expressed in atomic units are given by

$$-U_l^+(r) = -2\gamma V + \alpha^2 V^2 - \frac{3}{4} \frac{(\eta')^2}{\eta^2} + \frac{1}{2} \frac{\eta''}{\eta} + \frac{l+1}{r} \frac{\eta'}{\eta} \quad (13)$$

and

$$-U_l^-(r) = -2\gamma V + \alpha^2 V^2 - \frac{3}{4} \frac{(\eta')^2}{\eta^2} + \frac{1}{2} \frac{\eta''}{\eta} - \frac{l}{r} \frac{\eta'}{\eta}, \quad (14)$$

where  $\alpha$  is a fine-structure constant [not to be confused with the operator  $\alpha$  of Eq. (11)]. In Eqs. (12)–(14), the single prime corresponds to first-order derivative and the double primes to the second-order derivative with respect to  $r$ .

The proper solution of Eq. (12) behaves asymptotically as

$$g_l^\pm(K, r) \sim Kr [j_l(Kr) - \tan \delta_l^\pm n_l(Kr)], \quad (15)$$

where  $j_l$  and  $n_l$  are spherical Bessel functions of the first and second kind, respectively, and  $\delta_l^\pm$  are the phase shifts due to collisional interactions. The plus sign in  $\delta$  corresponds to the incident particles with spin up and the minus sign in  $\delta$  to those with spin down. The values of  $\delta_l^\pm$  may be obtained from Eq. (15). In the present calculation the wave functions  $g_l^\pm$  are obtained by numerical integration of Eq. (12) using the Numerov method and the spherical Bessel functions are evaluated as described in Ref. 12.

The generalized scattering amplitude for the collision process is given by<sup>13</sup>

$$A = f(K, \theta) + g(K, \theta) \boldsymbol{\sigma} \cdot \hat{\mathbf{n}}, \quad (16)$$

where

$$f(K, \theta) = \frac{1}{2iK} \sum_{l=0}^{\infty} \{ (l+1) [\exp(2i\delta_l^+) - 1] + l [\exp(2i\delta_l^-) - 1] \} P_l(\cos\theta), \quad (17a)$$

$$g(K, \theta) = \frac{1}{2K} \sum_{l=0}^{\infty} [\exp(2i\delta_l^+) - \exp(2i\delta_l^-)] P_l^1(\cos\theta), \quad (17b)$$

and  $\hat{\mathbf{n}}$  is the unit vector perpendicular to the scattering plane. The differential cross section (DCS) for the scattering of the spin- $\frac{1}{2}$  particles by the spin zero cadmium atoms is given by

$$\begin{aligned} \frac{d\sigma}{d\Omega} &= \sum_{\nu} |\langle \chi_{\nu} | A | \chi_{\nu} \rangle|^2 \\ &= |f|^2 + |g|^2 + (f^*g + fg^*) \hat{\mathbf{n}} \cdot \mathbf{P}_i, \end{aligned} \quad (18)$$

where  $\chi_{\nu}$  represents a spin state and  $\mathbf{P}_i = \langle \chi_{\nu} | \boldsymbol{\sigma} | \chi_{\nu} \rangle$  is the incident-beam polarization, which is zero in the present case. The integrated elastic cross section for the unpolarized incident beam can be obtained as

$$\sigma_{el} = 2\pi \int_0^{\pi} (|f|^2 + |g|^2) \sin\theta d\theta, \quad (19)$$

the momentum transfer cross section by

$$\sigma_M = 2\pi \int_0^{\pi} (1 - \cos\theta) [|f|^2 + |g|^2] \sin\theta d\theta, \quad (20)$$

and the total cross section by

$$\sigma_{tot} = \frac{2\pi}{K^2} \sum_{l=0}^{\infty} \{ (l+1) [1 - \text{Re}(S_l^+)] + l [1 - \text{Re}(S_l^-)] \}, \quad (21)$$

where  $S_l^\pm = \exp(2i\delta_l^\pm)$ .

Since the spin-orbit interaction is a short-range interaction, the phase shifts of the spin-up and the spin-down particles are equal ( $\delta_l^+ = \delta_l^-$ ) for large angular momenta  $l\hbar$ . Hence for large  $l$ ,  $g(\theta) = 0$  and the contribution to the scattering amplitude comes only from  $f(\theta)$ . If Born approximation is used for higher partial waves with  $l > M$ ,  $f(\theta)$  can be written as

$$\begin{aligned} f(K, \theta) &= \frac{1}{2iK} \sum_{l=0}^M [(l+1)(S_l^+ - 1) + l(S_l^- - 1)] P_l \\ &+ f_B(K, \theta) - \frac{1}{2iK} \sum_{l=0}^M (2l+1)(S_{Bl} - 1) P_l, \end{aligned} \quad (22)$$

where  $f_B$  is the Born amplitude,  $S_{Bl} = \exp(2i\delta_{Bl})$ , and  $\delta_{Bl}$  is the Born phase shift. In the present work, a large number (20 or more, depending on the impact energy) of exact phase shifts have been evaluated before using the Born approximation and hence the contribution due to Born approximation is found to be very small, except on the DCS values at the forward peak. Since at large distance the interaction potential  $V(r)$  is dominated by the long-range part  $V_{LR}(r) = -\alpha_d/2r^4$  of the polarization potential, the Born phase shift  $\delta_{Bl}$  and the amplitude  $f_B$  are obtained<sup>14</sup> using this term only.

The interaction between the electron or positron spin and the orbital angular momentum  $\mathbf{L}$ , which depends on the velocity and position vector with respect to the target atom, can cause the spin to orient. Hence, even with an unpolarized incident beam the orientations in a preferred direction can give a net spin polarization in the scattered beam. The amount of polarization produced due to the collision in the scattered beam is given by<sup>13</sup>

$$\mathbf{P}(\theta) = \frac{\langle A \chi_{\nu} | \boldsymbol{\sigma} | A \chi_{\nu} \rangle}{\langle A \chi_{\nu} | A \chi_{\nu} \rangle} = \frac{f^*g + fg^*}{|f|^2 + |g|^2} \hat{\mathbf{n}} = P(\theta) \hat{\mathbf{n}}. \quad (23)$$

The other two spin polarization parameters  $T$  and  $U$  giving the angle of the component of the polarization vector in the scattering plane are given by<sup>13</sup>

$$T(\theta) = \frac{|f|^2 - |g|^2}{|f|^2 + |g|^2}, \quad U(\theta) = i \frac{fg^* - gf^*}{|f|^2 + |g|^2}. \quad (24)$$

### III. RESULTS AND DISCUSSION

#### A. Electrons scattering from cadmium

The calculated differential cross section curves for the elastically scattered electrons by cadmium as well as the comparison with the available experimentally measured values<sup>1,2</sup> are shown in Figs. 1–3. In these figures the

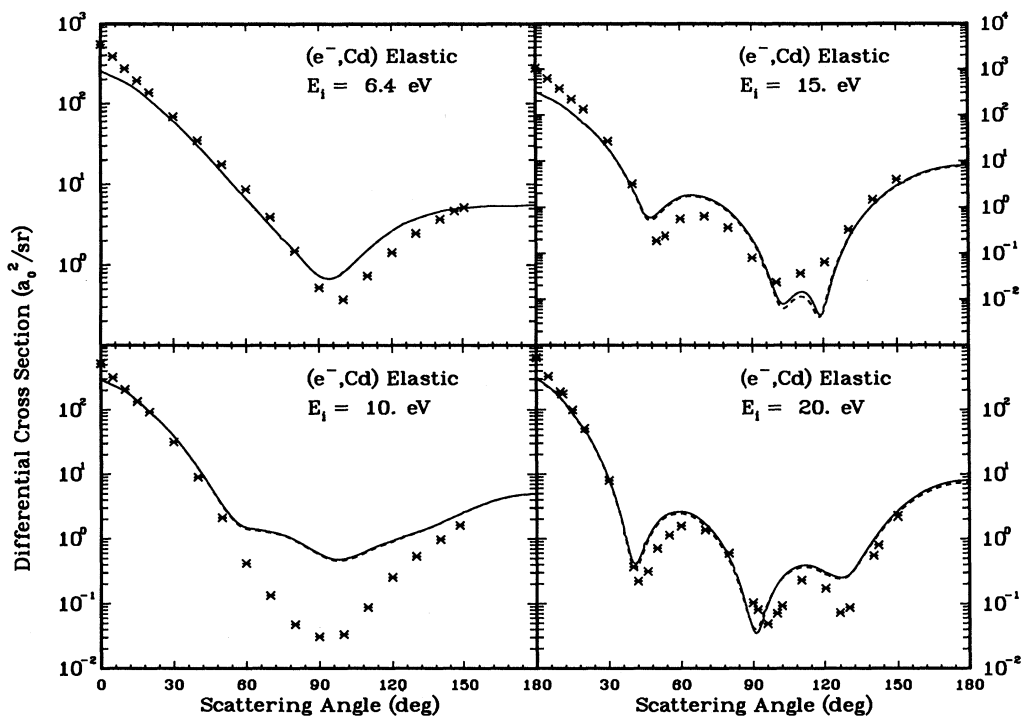


FIG. 1. Differential cross sections for elastic scattering of 6.4-, 10-, 15- and 20-eV electrons from cadmium in units of  $a_0^2 \text{sr}^{-1}$ : solid curves, present data obtained using the real potential in the Dirac equation; dashed curves, present data obtained using the complex potential in the Dirac equation; asterisks, experimental values from Ref. 2.

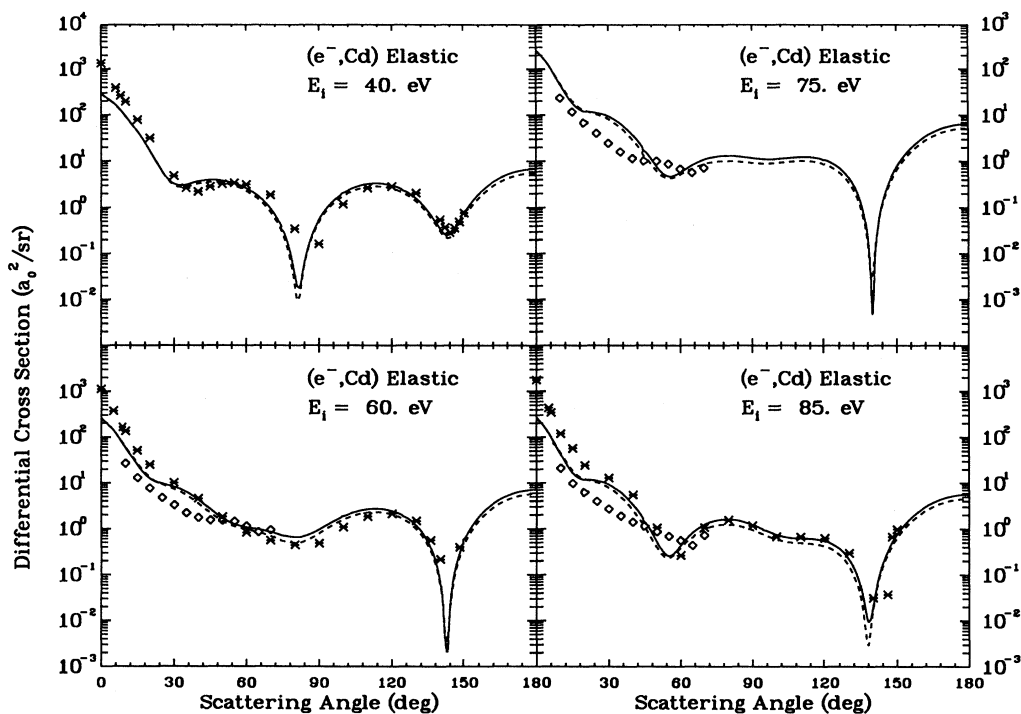


FIG. 2. Same as Fig. 1, but at impact energies of 40, 60, 75, and 85 eV: diamonds, experimental values from Ref. 1; and asterisks, those of Ref. 2.

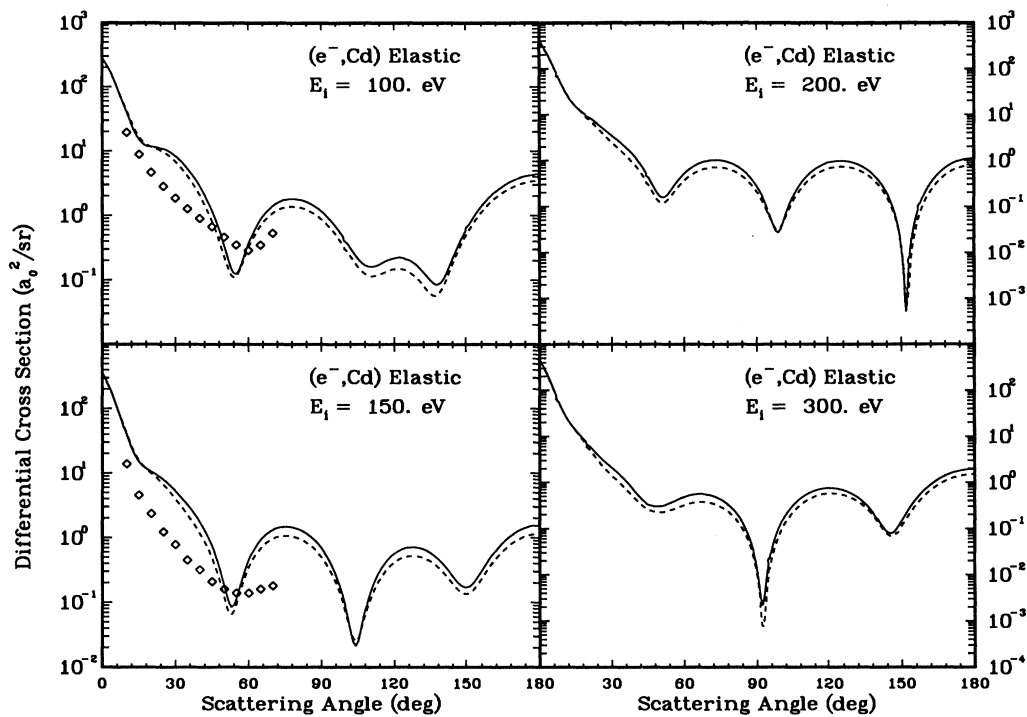


FIG. 3. Same as Fig. 1, but at impact energies of 100, 150, 200, and 300 eV: diamonds, experimental values from Ref. 1.

solid curves correspond to the DCS values obtained by representing the projectile-target interaction by the real model potential  $V_R(r)$  alone and the dashed curves correspond to those obtained by representing the interaction by the complex potential, that is, including the absorption potential. Comparison between the two calculated curves, the solid and the dashed, shows some differences, especially at the minima and maxima, at higher impact energies, while the difference is very small at the lowest considered energies. This is expected since at the lowest energies the scattering is mainly elastic and there is almost no effect of absorption on the DCS values at these energies, whereas at higher impact energies due to inelastic processes absorption shows some effect on the DCS curves, especially at the minima and maxima at larger scattering angles. The numerical values of the DCS using the complex model potential in the Dirac equation [Eq. (1)] are presented in Table I. Comparison of the present calculated DCS values with those obtained experimentally shown in Figs. 1–3 shows that, except at an electron impact energy of 10 eV, the shapes and features of the calculated DCS curves agree very well with the measured values of Ref. 2 at all other energies. The agreement is reasonable with those of Nogueira, Newell, and Johnstone.<sup>1</sup> The relative values of Ref. 2 have been normalized by multiplying by a factor which may be from 5 to 15 to fit the present calculated values. At electron impact energies 60 and 85 eV, where both Nogueira, Newell, and Johnstone<sup>1</sup> and Marinkovic<sup>2</sup> have carried out the experiment, the shapes and locations of the minima in the DCS values by Nogueira, Newell, and Johnstone, in general, do not agree well with those of Marinkovic and also with

those of the present calculation. The measured values of Ref. 1 below  $45^\circ$  of scattering angle at 85 eV agree better with the other calculated DCS values.<sup>3</sup> At 100 and 150 eV also the agreement of the measured values of Ref. 1 is better with the other calculated DCS values<sup>3</sup> than with the present results. However, their<sup>3</sup> calculated DCS curves at energies higher than 40 eV show a greater number of prominent maxima and minima at larger scattering angles, which are absent in the present calculated DCS curves as well as in the measured values of Ref. 2. These oscillations in the DCS curves in their work may have, in part, been caused by the calculation of fewer numbers of exact partial waves. In the present calculation a few errors may have been introduced, which can be explained as follows. The contributions from very large partial waves have been obtained by using the Born approximation, where only the long-range part of the polarization potential is used. Some improvement, though small, in the calculated values could have been achieved by including the other potentials such as the static and exchange in the Born approximation. Also, in the calculation using the complex potential, the correction terms in the Dirac equations have been calculated using only the real part of the potential. Inclusion of the absorption potential in these terms could have improved the results with complex potential by a small amount. Some discrepancy between the calculated and the measured values may have come from the uncertainty in the value of  $\alpha_d$  of the atomic dipole polarizability.

The values of the present integrated elastic cross sections are given in Table II, along with the calculated values of Ref. 3. The elastic cross sections obtained using

TABLE I. The differential cross section for elastic scattering of electrons by cadmium (in units of  $a_0^2\text{sr}^{-1}$ ) obtained using the complex potential in the Dirac equation. Impact energies are indicated. The notation  $a [b]$  for the cross sections means  $a \times 10^b$ .

| $\theta$<br>(deg) | $E_i$ (eV)=6.4 | 10       | 15       | 20       | 40       | 60       |
|-------------------|----------------|----------|----------|----------|----------|----------|
| 0                 | 2.59[2]        | 2.98[2]  | 3.17[2]  | 3.11[2]  | 2.90[2]  | 2.59[2]  |
| 5                 | 2.17[2]        | 2.39[2]  | 2.36[2]  | 2.22[2]  | 1.79[2]  | 1.40[2]  |
| 10                | 1.85[2]        | 1.92[2]  | 1.72[2]  | 1.50[2]  | 9.28[1]  | 6.08[1]  |
| 15                | 1.49[2]        | 1.38[2]  | 1.11[2]  | 8.62[1]  | 4.29[1]  | 2.62[1]  |
| 20                | 1.12[2]        | 9.35[1]  | 6.64[1]  | 4.69[1]  | 1.70[1]  | 1.33[1]  |
| 25                | 8.28[1]        | 6.21[1]  | 3.77[1]  | 2.18[1]  | 6.20     | 9.33     |
| 30                | 6.07[1]        | 3.90[1]  | 1.85[1]  | 7.95     | 3.05     | 7.27     |
| 35                | 4.35[1]        | 2.27[1]  | 7.51     | 2.01     | 2.78     | 5.31     |
| 40                | 3.03[1]        | 1.24[1]  | 2.45     | 3.59[-1] | 3.30     | 3.50     |
| 45                | 2.08[1]        | 6.39     | 6.61[-1] | 7.40[-1] | 3.53     | 2.19     |
| 50                | 1.42[1]        | 3.28     | 6.17[-1] | 1.65     | 3.42     | 1.44     |
| 55                | 9.63           | 1.87     | 1.09     | 2.29     | 2.96     | 1.11     |
| 60                | 6.62           | 1.42     | 1.56     | 2.43     | 2.28     | 9.60[-1] |
| 65                | 4.54           | 1.33     | 1.72     | 2.15     | 1.52     | 8.37[-1] |
| 70                | 3.09           | 1.24     | 1.54     | 1.55     | 8.03[-1] | 6.90[-1] |
| 75                | 2.15           | 1.12     | 1.21     | 9.58[-1] | 2.71[-1] | 5.46[-1] |
| 80                | 1.49           | 9.35[-1] | 7.97[-1] | 4.57[-1] | 2.07[-2] | 4.91[-1] |
| 85                | 1.00           | 7.27[-1] | 4.29[-1] | 1.50[-1] | 9.78[-2] | 5.62[-1] |
| 90                | 7.34[-1]       | 5.72[-1] | 1.88[-1] | 4.24[-2] | 4.83[-1] | 7.88[-1] |
| 95                | 6.74[-1]       | 4.75[-1] | 5.57[-2] | 8.04[-2] | 1.09     | 1.15     |
| 100               | 7.93[-1]       | 4.64[-1] | 1.00[-2] | 1.96[-1] | 1.77     | 1.59     |
| 105               | 1.09           | 5.21[-1] | 7.44[-3] | 3.04[-1] | 2.38     | 1.99     |
| 110               | 1.53           | 6.34[-1] | 1.14[-2] | 3.60[-1] | 2.76     | 2.25     |
| 115               | 2.04           | 7.69[-1] | 6.47[-3] | 3.45[-1] | 2.83     | 2.28     |
| 120               | 2.62           | 8.99[-1] | 8.01[-3] | 2.82[-1] | 2.57     | 2.04     |
| 125               | 3.20           | 1.06     | 5.83[-2] | 2.42[-1] | 2.02     | 1.57     |
| 130               | 3.71           | 1.23     | 2.16[-1] | 2.77[-1] | 1.36     | 9.74[-1] |
| 135               | 4.17           | 1.44     | 5.44[-1] | 4.93[-1] | 7.17[-1] | 4.12[-1] |
| 140               | 4.59           | 1.75     | 1.07     | 9.19[-1] | 3.04[-1] | 5.73[-2] |
| 145               | 4.88           | 2.12     | 1.83     | 1.60     | 2.45[-1] | 4.82[-2] |
| 150               | 5.05           | 2.57     | 2.80     | 2.51     | 6.12[-1] | 4.65[-1] |
| 155               | 5.23           | 3.09     | 3.88     | 3.56     | 1.38     | 1.28     |
| 160               | 5.36           | 3.62     | 5.01     | 4.71     | 2.43     | 2.39     |
| 165               | 5.37           | 4.11     | 6.08     | 5.76     | 3.57     | 3.61     |
| 170               | 5.36           | 4.52     | 6.91     | 6.65     | 4.60     | 4.69     |
| 175               | 5.46           | 4.79     | 7.49     | 7.22     | 5.31     | 5.43     |
| 180               | 5.54           | 4.88     | 7.73     | 7.37     | 5.56     | 5.77     |
| $\theta$<br>(deg) | $E_i$ (eV)=75  | 85       | 100      | 150      | 200      | 300      |
| 0                 | 2.59[2]        | 2.66[2]  | 2.85[2]  | 3.53[2]  | 4.03[2]  | 4.65[2]  |
| 5                 | 1.27[2]        | 1.24[2]  | 1.25[2]  | 1.33[2]  | 1.34[2]  | 1.27[2]  |
| 10                | 4.89[1]        | 4.52[1]  | 4.26[1]  | 4.02[1]  | 3.80[1]  | 3.24[1]  |
| 15                | 2.04[1]        | 1.84[1]  | 1.68[1]  | 1.57[1]  | 1.51[1]  | 1.29[1]  |
| 20                | 1.26[1]        | 1.22[1]  | 1.16[1]  | 9.86     | 8.39     | 5.89     |
| 25                | 1.04[1]        | 1.03[1]  | 9.62     | 6.56     | 4.59     | 2.63     |
| 30                | 8.17           | 7.82     | 6.91     | 3.94     | 2.49     | 1.39     |
| 35                | 5.36           | 4.88     | 4.13     | 2.22     | 1.43     | 7.91[-1] |
| 40                | 2.92           | 2.52     | 2.06     | 1.16     | 7.78[-1] | 4.20[-1] |
| 45                | 1.35           | 1.07     | 8.15[-1] | 4.83[-1] | 3.21[-1] | 2.58[-1] |
| 50                | 6.22[-1]       | 3.88[-1] | 2.35[-1] | 1.20[-1] | 1.24[-1] | 2.26[-1] |
| 55                | 4.27[-1]       | 2.33[-1] | 1.15[-1] | 9.52[-2] | 1.74[-1] | 2.57[-1] |
| 60                | 5.12[-1]       | 3.86[-1] | 3.17[-1] | 3.43[-1] | 3.53[-1] | 3.22[-1] |
| 65                | 6.97[-1]       | 6.83[-1] | 6.95[-1] | 6.90[-1] | 5.46[-1] | 3.74[-1] |
| 70                | 8.72[-1]       | 9.80[-1] | 1.08     | 9.63[-1] | 6.77[-1] | 3.66[-1] |
| 75                | 9.75[-1]       | 1.18     | 1.33     | 1.07     | 7.01[-1] | 2.93[-1] |
| 80                | 1.01           | 1.23     | 1.36     | 9.96[-1] | 6.05[-1] | 1.83[-1] |
| 85                | 9.82[-1]       | 1.14     | 1.18     | 7.82[-1] | 4.19[-1] | 7.66[-2] |

TABLE I. (Continued).

| (deg) \ $E_i$ (eV)=75 | 85       | 100      | 150      | 200      | 300      |          |
|-----------------------|----------|----------|----------|----------|----------|----------|
| 90                    | 9.30[-1] | 9.46[-1] | 8.79[-1] | 5.01[-1] | 2.14[-1] | 9.39[-3] |
| 95                    | 8.99[-1] | 7.43[-1] | 5.60[-1] | 2.39[-1] | 6.83[-2] | 1.13[-2] |
| 100                   | 9.18[-1] | 5.91[-1] | 3.08[-1] | 6.84[-2] | 3.48[-2] | 9.13[-2] |
| 105                   | 9.72[-1] | 5.15[-1] | 1.62[-1] | 2.74[-2] | 1.23[-1] | 2.31[-1] |
| 110                   | 1.02     | 4.92[-1] | 1.16[-1] | 1.08[-1] | 2.99[-1] | 3.88[-1] |
| 115                   | 9.97[-1] | 4.73[-1] | 1.27[-1] | 2.61[-1] | 5.02[-1] | 5.16[-1] |
| 120                   | 8.73[-1] | 4.15[-1] | 1.48[-1] | 4.16[-1] | 6.65[-1] | 5.74[-1] |
| 125                   | 6.38[-1] | 3.00[-1] | 1.40[-1] | 5.11[-1] | 7.32[-1] | 5.43[-1] |
| 130                   | 3.49[-1] | 1.51[-1] | 1.01[-1] | 5.12[-1] | 6.80[-1] | 4.33[-1] |
| 135                   | 1.01[-1] | 2.86[-2] | 6.06[-2] | 4.24[-1] | 5.27[-1] | 2.80[-1] |
| 140                   | 2.84[-3] | 1.77[-2] | 7.76[-2] | 2.91[-1] | 3.20[-1] | 1.40[-1] |
| 145                   | 1.60[-1] | 2.02[-1] | 2.18[-1] | 1.75[-1] | 1.28[-1] | 6.95[-2] |
| 150                   | 6.34[-1] | 6.33[-1] | 5.28[-1] | 1.35[-1] | 1.45[-2] | 1.12[-1] |
| 155                   | 1.40     | 1.30     | 1.01     | 2.06[-1] | 1.73[-2] | 2.82[-1] |
| 160                   | 2.38     | 2.14     | 1.64     | 3.86[-1] | 1.38[-1] | 5.59[-1] |
| 165                   | 3.42     | 3.02     | 2.30     | 6.37[-1] | 3.39[-1] | 8.89[-1] |
| 170                   | 4.37     | 3.80     | 2.90     | 8.93[-1] | 5.57[-1] | 1.20     |
| 175                   | 5.01     | 4.35     | 3.30     | 1.08     | 7.24[-1] | 1.42     |
| 180                   | 5.17     | 4.60     | 3.41     | 1.17     | 7.84[-1] | 1.50     |

the pure real potential in the present work are slightly larger than those obtained using the complex potential at all energies considered. This is in general to be expected since inclusion of absorption reduces the elastically scattered beam and hence decreases the elastic cross sections. Comparing the present elastic cross sections with the oth-

er calculated<sup>3</sup> values in Table II, we see a large difference between them. The values of the present cross section fall more smoothly with higher impact energies than those of Ref. 3, where there is a sharp fall in values from 40 to 60 eV. The difference in the two calculations could have come from the difference in forms of model polar-

TABLE II. Integrated elastic and total cross sections (in units of  $a_0^2$ ) for *electron* and *positron* scattering by cadmium. The letters within parentheses indicate the type of potential used in the Dirac equation: *R*, real potential and *C*, complex potential.

| $E_i$<br>(eV) | $(e^-, \text{Cd})$ |                      |        | $(e^+, \text{Cd})$               |          |                      |        |                                  |
|---------------|--------------------|----------------------|--------|----------------------------------|----------|----------------------|--------|----------------------------------|
|               | Present            | $\sigma_{\text{el}}$ | Ref. 4 | $\sigma_{\text{tot}}$<br>Present | Present  | $\sigma_{\text{el}}$ | Ref. 4 | $\sigma_{\text{tot}}$<br>Present |
| 6.4           | 177.26(R)          |                      |        |                                  | 93.58(R) |                      |        |                                  |
|               | 176.98(C)          |                      |        | 177.58(C)                        | 91.99(C) |                      |        | 97.84(C)                         |
| 10            | 122.23(R)          |                      |        |                                  | 64.55(R) |                      |        |                                  |
|               | 121.26(C)          |                      |        | 133.44(C)                        | 61.50(C) |                      |        | 72.90(C)                         |
| 15            | 86.60(R)           |                      |        |                                  | 46.32(R) |                      |        |                                  |
|               | 84.80(C)           |                      |        | 88.94(C)                         | 42.66(C) |                      |        | 58.44(C)                         |
| 20            | 69.76(R)           |                      |        |                                  | 36.98(R) |                      |        |                                  |
|               | 67.30(C)           |                      |        | 72.92(C)                         | 33.43(C) |                      |        | 51.13(C)                         |
| 40            | 53.44(R)           |                      | 95.03  |                                  | 22.52(R) |                      | 78.85  |                                  |
|               | 49.90(C)           |                      |        | 57.30(C)                         | 19.55(C) |                      |        | 42.53(C)                         |
| 60            | 43.35(R)           |                      | 29.03  |                                  | 17.32(R) |                      | 24.28  |                                  |
|               | 40.43(C)           |                      |        | 47.61(C)                         | 15.62(C) |                      |        | 39.07(C)                         |
| 75            | 36.81(R)           |                      | 26.99  |                                  | 15.09(R) |                      | 21.27  |                                  |
|               | 33.96(C)           |                      |        | 40.97(C)                         | 15.39(C) |                      |        | 36.41(C)                         |
| 85            | 33.92(R)           |                      | 26.11  |                                  | 14.00(R) |                      | 19.98  |                                  |
|               | 31.04(C)           |                      |        | 37.94(C)                         | 14.44(C) |                      |        | 34.39(C)                         |
| 100           | 31.20(R)           |                      | 20.86  |                                  | 12.73(R) |                      | 16.15  |                                  |
|               | 28.26(C)           |                      |        | 34.98(C)                         | 13.58(C) |                      |        | 32.44(C)                         |
| 150           | 27.07(R)           |                      | 19.01  |                                  | 10.25(R) |                      | 13.67  |                                  |
|               | 24.15(C)           |                      |        | 30.13(C)                         | 11.41(C) |                      |        | 27.60(C)                         |
| 200           | 24.56(R)           |                      |        |                                  | 8.96(R)  |                      |        |                                  |
|               | 21.86(C)           |                      |        | 27.14(C)                         | 10.03(C) |                      |        | 24.50(C)                         |
| 300           | 20.62(R)           |                      |        |                                  | 7.50(R)  |                      |        |                                  |
|               | 18.40(C)           |                      |        | 22.68(C)                         | 8.93(C)  |                      |        | 20.72(C)                         |

TABLE III. Momentum-transfer cross sections  $\sigma_M$  (in units of  $a_0^2$ ) for elastic scattering of electrons and positrons from cadmium at various electron impact energies  $E_i$ . The type of potential used in the Dirac equation is shown within parentheses.

| $E_i$<br>(eV) | $(e^-, \text{Cd})$ |         | $(e^+, \text{Cd})$ |
|---------------|--------------------|---------|--------------------|
|               | Real               | Complex | Real               |
| 6.4           | 53.28              | 53.11   | 24.99              |
| 10            | 25.67              | 25.28   | 15.86              |
| 15            | 18.40              | 17.69   | 11.62              |
| 20            | 17.87              | 16.70   | 9.60               |
| 40            | 24.29              | 20.88   | 6.36               |
| 60            | 21.27              | 17.86   | 4.89               |
| 75            | 15.82              | 12.94   | 4.20               |
| 85            | 13.14              | 10.54   | 3.85               |
| 100           | 10.63              | 8.29    | 3.46               |
| 150           | 7.77               | 5.80    | 2.71               |
| 200           | 6.90               | 5.14    | 2.27               |
| 300           | 5.69               | 4.31    | 1.74               |

ization potentials used and the difference in defining the direct potential in the exchange potential, and from the difference in the Schrödinger equation and Dirac equation which contains the spin-orbit interaction term along with relativistic correction terms. The other main difference may have come from their fewer number of exact partial waves compared to the present calculation before taking the approximation for the higher partial waves. Though these differences are not expected to make the large difference in the cross-section values be-

tween the two calculations, a better judgment can be made when some more calculated and absolute experimental data become available. The values of the total cross section for electrons scattering from cadmium are also presented in Table II. The tabular values show a decrease in the cross-section values with increasing impact energies. No other measured or calculated values are available for comparison.

The momentum transfer cross sections obtained using the real potential as well as the complex potential for the elastic scattering of electrons from cadmium are presented in Table III. In the energy range considered, the values of the cross sections obtained using both the real and complex potentials show a minimum at 20 eV. Similar to the case of integrated elastic cross sections the values of  $\sigma_M$  obtained using the real potential are a little higher than those obtained using the complex potential. Again, the reduction in the values of the momentum transfer cross section is due to inclusion of absorption.

The calculated values of the spin polarization  $P$  for the elastic scattering of electrons from cadmium at various impact energies are shown in Figs. 4–6. Like the DCS figures, the solid curves correspond to the values obtained using the pure real potential and the dashed curves to those obtained using the complex potential in the Dirac equation. At all energies both these curves show little difference between them, except at some minima and maxima where inclusion of absorption causes the minima to go deeper and the maxima to peak higher in general. Figures 4–6 show a significant amount of spin polariza-

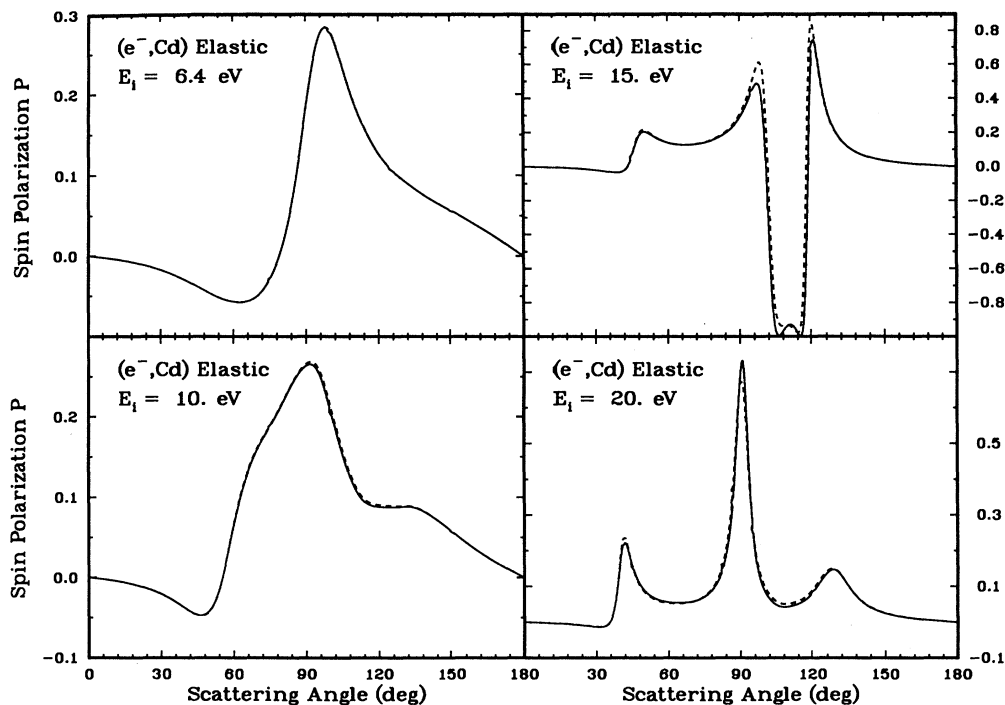


FIG. 4. The spin polarization  $P$  for elastic scattering of 6.4-, 10-, 15-, and 20-eV electrons from cadmium: solid curves, present data obtained using real potential in the Dirac equation; and dashed curves, present data obtained using complex potential in the Dirac equation.



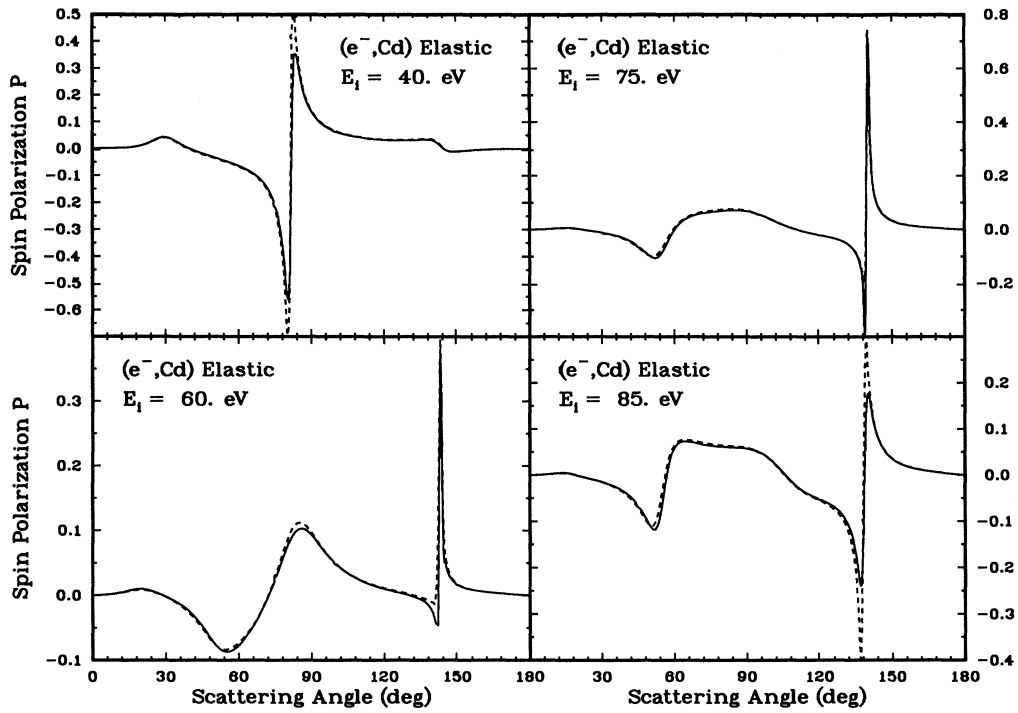


FIG. 5. Same as Fig. 4, but at impact energies of 40, 60, 75, and 85 eV.

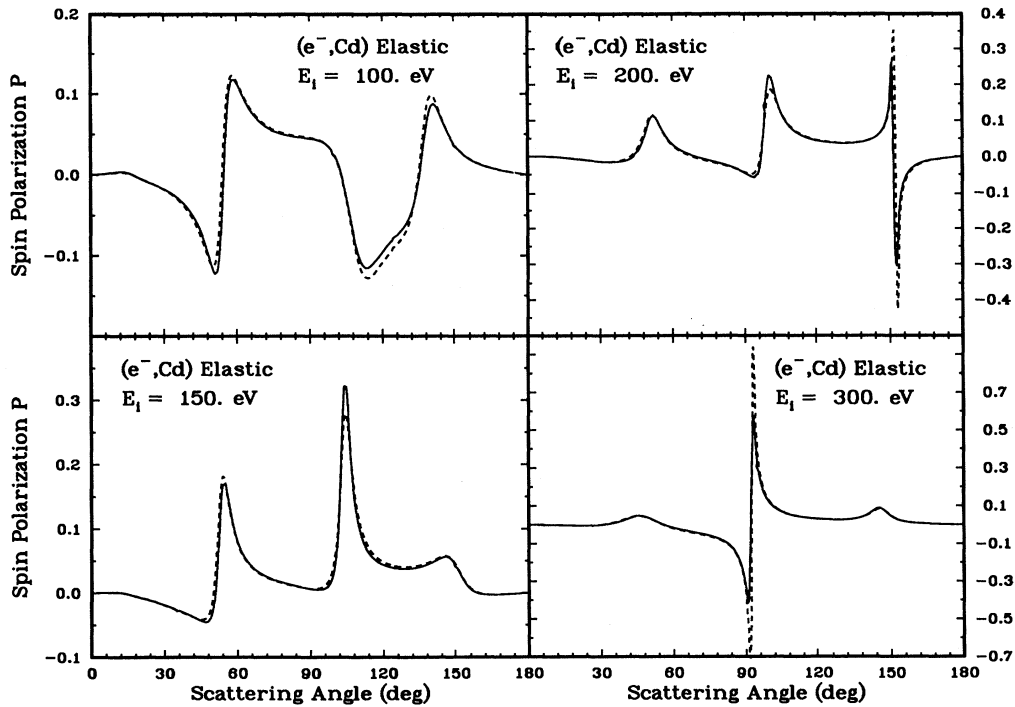


FIG. 6. Same as Fig. 4, but at impact energies of 100, 150, 200, and 300 eV.

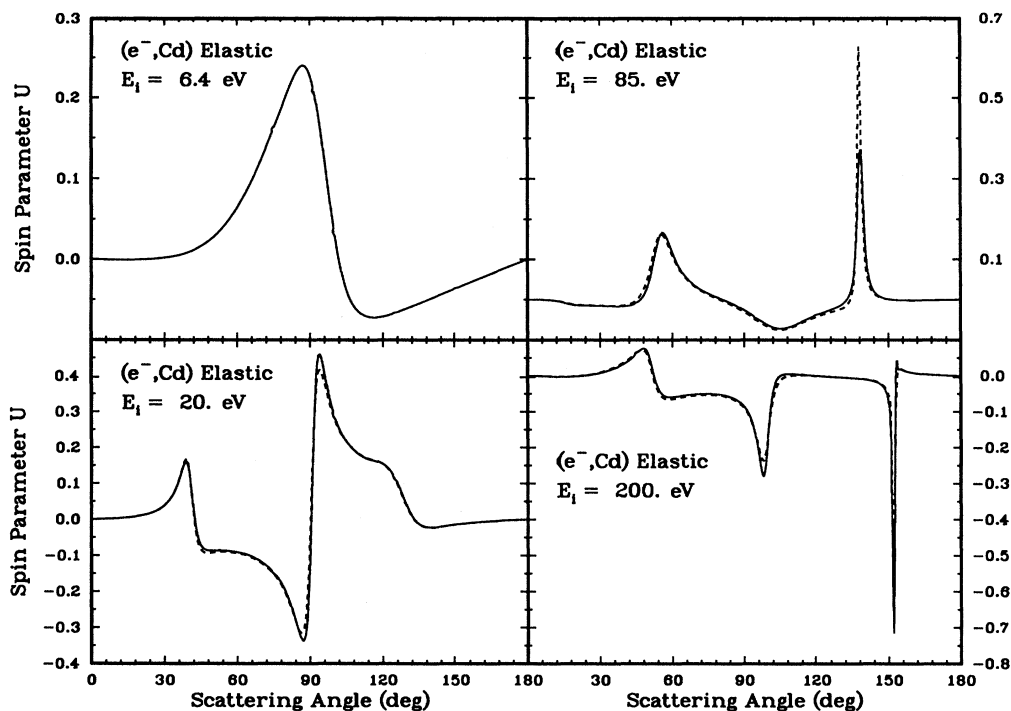


FIG. 7. The spin polarization parameter  $U$  for elastic scattering of 6.4-, 20-, 85-, and 200-eV electrons from cadmium: solid curves, present data obtained using real potential in the Dirac equation; dashed curves, present data obtained using complex potential in the Dirac equation.

tion in the scattered beam at various scattering angles. This indicates that it will be of much interest to carry out experiments to measure the spin polarization of the electron beam scattered by cadmium atoms. There have been a number of spin-polarization measurements<sup>15</sup> of the closed-shell argon atom. The measurement of the polarization parameters  $T$  and  $U$  are difficult to carry out. The parameter  $U$  is shown only for a few energies in Fig. 7, which shows features similar to the polarization curves.

### B. Positrons scattering from cadmium

The differential cross sections for the elastic scattering of positrons from cadmium at all impact energies considered are shown in Figs. 8–10. In these figures, also, the solid curves represent the DCS without absorption, while the dashed curves represent the DCS with absorption. It can be observed from Figs. 8–10 that the DCS curves, especially the solid curves, for positrons scattering show comparatively fewer features than those for the electrons scattering. In case of positrons scattering, the solid curves show one prominent minimum, which occurs at all energies considered here, and one shallow minimum, which tends to disappear at the lower and higher impact energies. The fewer features in the positron DCS curves can be understood in terms of the weaker interaction (cancellation of the repulsive static potential and attractive polarization potential, and no exchange) of the positrons with the target, causing weaker interference with the inner atomic electrons. The lowest

impact energy, 6.4 eV, considered is higher from the positron-cadmium inelastic-scattering threshold energy, 2.191 eV, than from the electron-cadmium inelastic-scattering threshold energy. Hence the effect of absorption, which increases with higher impact energy, can be seen at all energies in Figs. 8–10. From these figures we see that at lower energies, 20 eV or less, both the solid and the dotted curves for the elastic scattering of positrons remain close to each other in features and values. However, with higher impact energies 40 eV and up, the solid and dashed DCS curves start to show a difference in the location and value of the first prominent minimum and shape of the DCS curves at larger scattering angles. However, both curves peak about the same in the forward direction at all energies. In the solid DCS curves, the first minimum shifts consistently toward smaller scattering angles with higher impact energies and at larger scattering angles the DCS values decrease monotonically. The dashed curves differ significantly from the solid curves and show a large minimum at high impact energies ( $> 150$  eV). Judging from the two curves, the solid and the dashed, the elastic scattering results obtained without the absorption may seem more reasonable than those obtained including the absorption. The monotonic decrease of the solid DCS values at larger scattering angles with higher impact energies is similar in nature to the observed values for positrons scattering from the closed-shell atom argon by Hyder *et al.*<sup>16</sup> When compared to the other calculation,<sup>3</sup> Ref. 3 shows features different from the present results and a higher number of

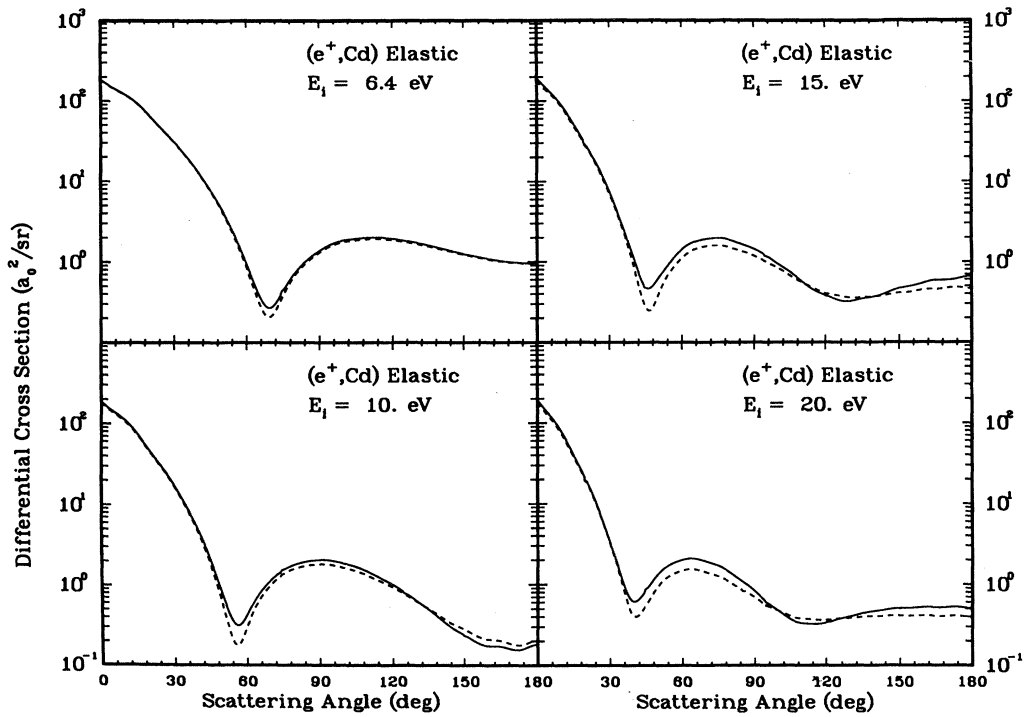


FIG. 8. Differential cross sections for elastic scattering of 6.4-, 10-, 15- and 20-eV positrons from cadmium in units of  $a_0^2 \text{sr}^{-1}$ : solid curves, present data obtained using real potential in the Dirac equation; dashed curves, present data obtained using complex potential in the Dirac equation.

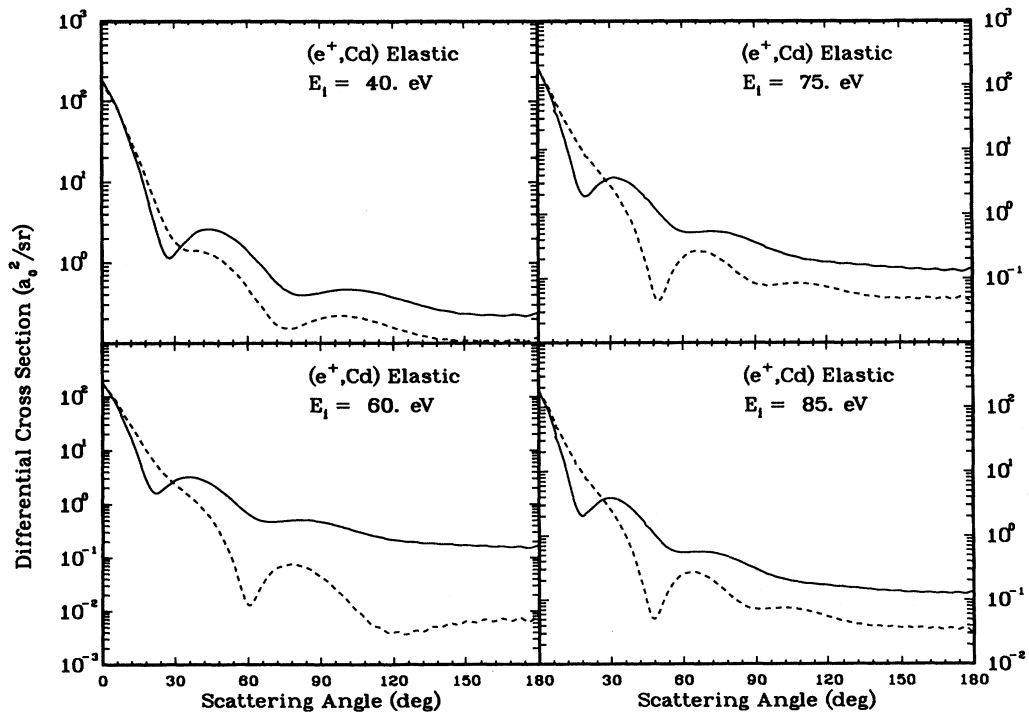


FIG. 9. Same as Fig. 8, but at impact energies of 40, 60, 75, and 85 eV.

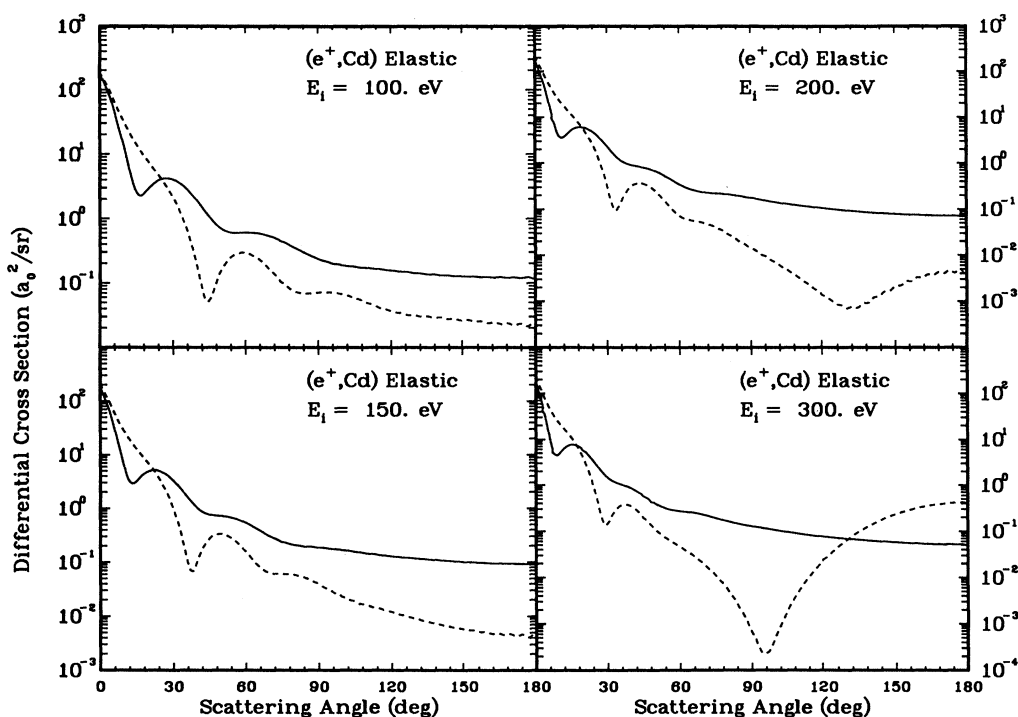


FIG. 10. Same as Fig. 8, but at impact energies of 100, 150, 200, and 300 eV.

minima and maxima in the DCS curves for positron scattering.

The form of the absorption potential used in the present work was derived by Staszewska, Schwenke, and Truhlar<sup>9</sup> for electrons scattering by treating the target as a homogeneous free-electron gas system. The approach of their calculation suggests that the same potential can be used for positrons scattering as well. However, the present results indicate that in the case of absorption the positron-target system may behave differently from the electron-target system, similar to the case of polarization. Since the two projectiles distort the target differently in the very near region,<sup>6</sup> the forms of the polarization potential are also different in that region. The various potentials for both electrons and positrons scattering from cadmium at energies of 15 and 75 eV are shown in Fig. 11. The curves represent the absolute values of the potentials. Hence, for the electron case, all the potential values are negative, and for the positron case, all the potential values are negative except the static potential (solid curves). The figure shows that the polarization potential (dotted curve) is the most dominating one at a large distance for both electron and positron scattering. The absorption potential (dashed curves) behaves in the same manner in both cases, except for the positrons it turns on a little earlier and becomes much stronger at a smaller distance with higher impact energy (> 60 eV) and may cause the inconsistency in the DCS curves. This strong peak in the absorption potential right after it turns on at higher energy seems rather unusual, since at higher energies the probability of positronium formation in gen-

eral decreases and hence the potential should not become unusually strong.

The values of the integrated elastic cross sections, obtained by representing the projectile-target interaction both by the real potential and the complex potential, for elastic scattering of positrons from cadmium are presented in Table II. Cross sections obtained in both ways show a smooth decrease in value with higher impact energies. The cross-sectional values obtained using the real potential are higher than those obtained using the complex potential at impact energies below 75 eV, from which energy the former values are smaller than the latter. This can be explained as we look at the DCS curves at higher impact energies in Figs. 9 and 10. For the dashed curves, larger contributions come from the slow decrease of the DCS values near the forward direction. As explained above there seems to be some inconsistency in the integrated elastic cross sections obtained using the complex potential at higher impact energies for positrons scattering from cadmium. As in the case of electron scattering, comparison with Ref. 3 shows that the present cross sections differ in values and in the rate of decrease at higher impact energies with those of Ref. 3. Their values suggest a sharp decrease in cross section between 40 and 60 eV, after which the cross section falls slowly. The difference can be explained by the same reasons mentioned above for the electrons scattering. The total cross sections for the positrons scattering from cadmium are also presented in Table II. As in the case of integrated elastic cross sections, the total cross sections also decrease smoothly with higher impact energies in the

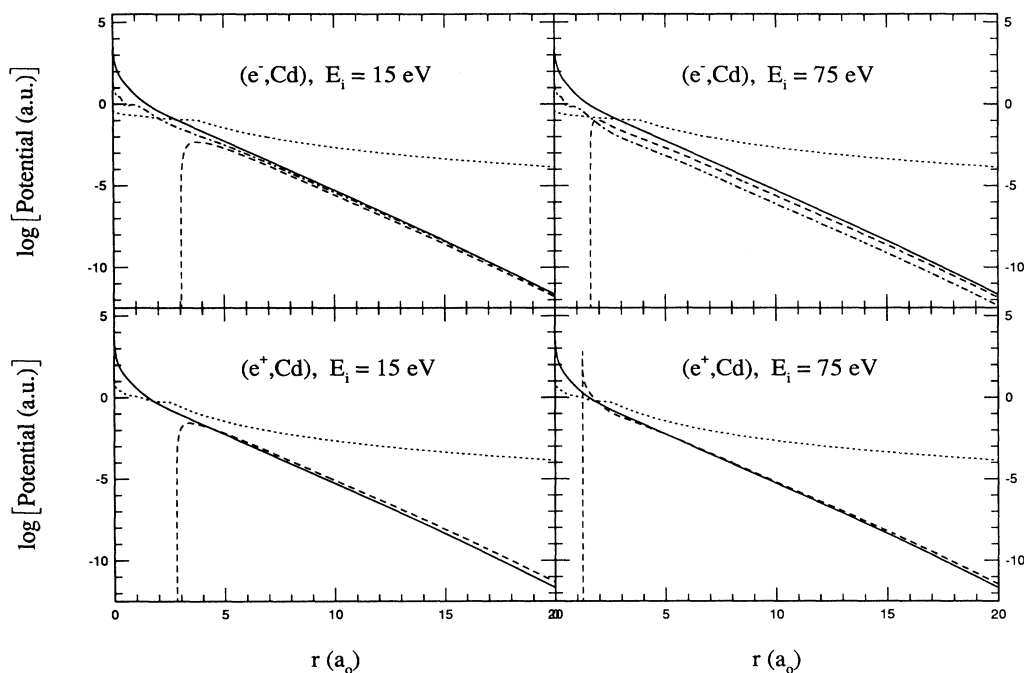


FIG. 11. Various interacting potentials  $V_S$  (solid),  $V_p$  (dotted),  $V_{ex}$  (dot-dashed), and  $V_A$  (dashed) in  $\log^{10}$  for  $e^\pm$  scattering from Cd at energies of 15 and 75 eV. The curves represent the absolute values of the potentials which are all negative except  $V_S$  of positrons which are positive.

impact energy range considered. No other calculation or experiment have been carried out for these values.

The momentum-transfer cross sections for the elastic scattering of positrons from cadmium obtained using only the real potential are presented in Table III. The values obtained using the complex potential have been omitted due to the apparent inconsistency in the absorption potential. The values of the cross section obtained using the real potential show a slow decrease with increasing impact energies.

Unlike the case of electrons scattering from cadmium, positrons scattering from cadmium show a negligible amount of polarization in the scattered beam. Hence these results are not presented here. The reason for smaller spin polarization, which depends on the spin-orbit interaction as well as on the spatial interaction potential, is probably due to the much weaker interaction between the positrons and cadmium atoms.

### C. Conclusions

Pure elastic and the total scattering of electrons and positrons from cadmium have been treated relativistically by solving the Dirac equation, where the projectile-target interaction has been represented by both the real and the complex model potentials. The features of the present calculated values of differential cross sections for the elas-

tic scattering of electrons from cadmium show good agreement with the recent measured<sup>2</sup> values of DCS, while agreement with the previous measured<sup>1</sup> DCS values is reasonable. The features of the present DCS curves and the values of the integrated cross sections for elastic scattering of electrons from cadmium show differences with the only other available calculation. The use of an absorption potential produces consistent results for both the elastic and the total scattering of electrons from cadmium. Electrons scattering from cadmium show a significant amount of spin polarization. The DCS curves for positrons scattering from cadmium have fewer features than those for electrons scattering. The use of the model absorption potential for positrons scattering from cadmium shows some inconsistency at higher energies. The spin polarization is found to be negligible for positrons scattering from cadmium.

### ACKNOWLEDGMENTS

This work has been carried out using the computer facilities at Georgia State University and at the Ohio State University. The author would like to thank Dr. B. Marinkovic for sending the experimental values of DCS for electron scattering from cadmium prior to final publication.

- <sup>1</sup>J. C. Nogueira, W. R. Newell, and W. M. Johnstone, *J. Phys. B* **20**, L537 (1987).
- <sup>2</sup>B. Marinkovic, V. Pejcev, D. Filipovic, and L. Vuskovic, in *Abstracts of the Contributed Papers, Fifteenth International Conference on the Physics of Electronic and Atomic Collisions, Brighton, 1987*, edited by J. Geddes, M. B. Gillbody, A. E. Kingston, and C. J. Latimer (Queen's University, Belfast, 1978), p. 186; B. Marinkovic, Ph.D. thesis, University of Belgrade, 1988.
- <sup>3</sup>A. W. Pangantiwar and R. Srivastava, *Phys. Rev. A* **40**, 2346 (1989).
- <sup>4</sup>E. Clementi and C. Roetti, *At. Data Nucl. Data Tables* **14**, 177 (1974).
- <sup>5</sup>J. K. O'Connell and N. F. Lane, *Phys. Rev. A* **27**, 1893 (1983).
- <sup>6</sup>A. Jain, in *Annihilation in Gases and Galaxies*, edited by R. Drachman (Goddard Space Flight Center, Greenbelt, MD, 1989), p. 71.
- <sup>7</sup>M. E. Riley and D. G. Truhlar, *J. Chem. Phys.* **63**, 2182 (1975).
- <sup>8</sup>Values are evaluated using tables of C. E. Moore, *Atomic Energy Levels*, Natl. Bur. Stand. (U.S.) Circ. No. 467 (U.S. GPO, Washington, D.C., 1949).
- <sup>9</sup>G. Staszewska, D. W. Schwenke, and D. G. Truhlar, *Phys. Rev. A* **29**, 3078 (1984).
- <sup>10</sup>See, for example, H. A. Bethe and E. E. Salpeter, *Quantum Mechanics of One- and Two-Electron Atoms* (Plenum/Rosetta, New York, 1977).
- <sup>11</sup>Sultana N. Nahar and J. M. Wadehra, *Phys. Rev. A* **43**, 1275 (1991).
- <sup>12</sup>Sultana N. Nahar and J. M. Wadehra, *Phys. Rev. A* **35**, 2051 (1987).
- <sup>13</sup>See, for example, C. J. Joachain, *Quantum Collision Theory* (North-Holland, Amsterdam, 1983), Chap. 18.
- <sup>14</sup>J. M. Wadehra and Sultana N. Nahar, *Phys. Rev. A* **36**, 1458 (1987).
- <sup>15</sup>J. Mehr, *Z. Phys.* **198**, 345 (1967); K. Schackert, *ibid.* **213**, 316 (1968); M. J. M. Beerlage, Z. Qing, and M. J. Van der Wiel, *J. Phys. B* **14**, 4627 (1981).
- <sup>16</sup>G. M. A. Hyder, M. S. Dababneh, Y. -F. Hsieh, W. E. Kaupila, C. K. Kwan, M. Mahdavi-Hezaveh, and T. S. Stein, *Phys. Rev. Lett.* **57**, 2252 (1986).